PCCP

PAPER

View Article Online
View Journal | View Issue

Cite this: *Phys. Chem. Chem. Phys.*, 2014, **16**, 11481

A combined computational and experimental study of the $[Co(bpy)_3]^{2+/3+}$ complexes as one-electron outer-sphere redox couples in dye-sensitized solar cell electrolyte media†

Narges Yaghoobi Nia,[a] Pooria Farahani,[b] Hassan Sabzyan,*[c] Mahmoud Zendehdel[c] and Mohsen Oftadeh[a]

Received 29th November 2013,
Accepted 16th April 2014

DOI: 10.1039/c3cp55034f

www.rsc.org/pccp

A combined experimental and computational investigation conducted to understand the nature of the interactions between cobalt II/III redox mediators ($[Co(bpy)_3]^{2+/3+}$) and their impact on the performance of the corresponding dye-sensitized solar cells (DSCs) is reported. The fully optimized equilibrium structures of cobalt(II/III)-tris-bipyridine complexes in the gas phase and acetonitrile solvent are obtained by the density functional B3LYP method using LanL2DZ and 6-31G(d,p) basis sets. The harmonic vibrational frequencies, infrared intensities and Raman scattering activities of the complexes are also calculated. The scaled computational vibrational wavenumbers show very good agreement with the experimental values. Calculations of the electronic properties of the complexes are also performed at the TD-B3LYP/6-31G(p,d)[LanL2DZ] level of theory. Detailed interpretations of the infrared and Raman spectra of the complexes in different phases are reported. Detailed atomic orbital coefficients of the frontier molecular orbitals and their major contributions to electronic excitations of the complexes are also reported. These results are in good agreement with the experimental electrochemical values. Marcus diagram is derived for the electron transfer reaction Co(II) + $D35^+$ → Co(III) + D35 using the Co–N bond length as a reaction coordinate.

1. Introduction

Dye-sensitized solar cells (DSCs) are promising hybrid/organic photovoltaic devices for high-efficiency, low-cost solar energy conversion.[1–3] In typical DSCs, a mesoporous film of TiO_2 nanoparticles is sensitized with light-harvesting dyes, either organic or metallorganic, which in most applications are surrounded by a redox mediator in an organic solvent, usually acetonitrile.[4–6] Classically, the I_3^-/I^- redox couple is used as a mediator in DSCs, which in conjunction with Ru(II) dyes delivers efficiencies around 11.4%.[7]

This redox system can be coupled to fully organic dyes with efficiencies exceeding 10%.[8] The I_3^-/I^- redox couple, however, has limitations due to its complex redox chemistry and its corrosive nature, which complicates large-scale DSC production.[9–11] Because of high voltage loss during the dye-regeneration reaction, the use of an I_3^-/I^- electrolyte as a redox shuttle limits the attainable open-circuit potential, V_{oc}, from 0.7 to 0.8 V and is thus a drawback of current DSC embodiments. This has prevented substantial gains in the power conversion efficiency (PCE) over the last 5 years.[10] To further improve the PCE, development of redox mediators exhibiting higher reduction potentials than that of the I_3^- ion is necessary. The cobalt(II/III)tris(bipyridyl), $[Co(bpy)_3]^{+2/+3}$, complexes have this property. However, such one-electron, outer-sphere redox couples often yield shorter electron lifetimes when used in the DSC. This faster interfacial charge recombination, when compared with (iodide/triiodide)-based redox electrolytes, lowers the photovoltage and reduces the efficiency of charge collection, hence decreasing the short circuit photocurrent density (J_{sc}) and the PCE.[12–14] Several promising results have been obtained using Co(II)/Co(III) redox mediators with organic dyes and different semiconductor systems as photoanodes.[15–17] A Zn(II)-porphyrin/organic dye cocktail in conjunction with $[Co(bpy)_3]^{2+/3+}$ provided the new liquid-based DSCs that record an efficiency of ~12.3% under AM1.5G conditions.[18]

Another interesting and largely unexplored aspect in DSCs based on cobalt electrolytes concerns the oxidized dye regeneration mechanism by Co(II) ions. The Co(II) complexes, having a d^7 electronic configuration, are characterized by two low-lying

[a] *Chemistry Department, Payame Noor University, 19395-4697 Tehran, I.R. Iran*
[b] *Department of Chemistry – Ångström, The Theoretical Chemistry Programme, Uppsala University, P.O. Box 518, SE-75120, Uppsala, Sweden*
[c] *Department of Chemistry, University of Isfahan, Isfahan 81746-73441, I.R. Iran. E-mail: sabzyan@sci.ui.ac.ir; Fax: +98-311-668-9732; Tel: +98-311-7932749*

† Electronic supplementary information (ESI) available. See DOI: 10.1039/c3cp55034f

electronic states of different spin-multiplicities, *i.e.*, the doublet and quartet states. The low-spin (LS) doublet state, ^{2}Co(II), has a $(t_{2g})^6(e_g)^1$ electron configuration, while the quartet high-spin (HS) state, ^{4}Co(II), has a $(t_{2g})^5(e_g)^2$ electronic configuration.[19] Co(III) complexes, with d^6 electron configuration, are generally LS, with the triplet state lying at higher energy. At room temperature the $[Co(bpy)_3]^{2+}$ complex is mainly present in its HS state.[19,20] However, when $[Co(bpy)_3]^{2+}$ is incorporated into zeolite-Y supercages[21–23] or into the cavities of three-dimensional oxalate networks,[24,25] the LS state becomes the ground state and the complex exhibits a spin crossover. Since dye regeneration consists of electron transfer from the ^{2,4}Co(II) complexes to the oxidized dye, giving the Co(III) complex, both HS and LS Co(II) could, in principle, contribute to the dye regeneration reaction pathway. Moreover, evaluation of the reorganization energy (λ) of the HS and LS species can be useful to estimate the kinetics of the regeneration process, described in the Marcus theory framework.[26,27]

Electron-transfer processes concerning oxidation of ^{2,4}Co(II) to Co(III) complexes in solution have been experimentally and computationally investigated in several studies.[28–31] Also, significant theoretical and experimental efforts have been performed to understand the self-exchange reaction of the $[Co(NH_3)_6]^{2+/3+}$ complexes.[32,33] Mosconi *et al.* reported a combined experimental and computational investigation to understand the nature of the interactions between cobalt redox mediators and TiO_2 surfaces sensitized by ruthenium and organic dyes, and worked out their impact on the performance of the corresponding DSC.[31]

Motivated by the great interest in full exploitation of the potential of cobalt-based electrolytes in the DSC framework, in the present study, we report a combined experimental and computational investigation to understand the nature of the electron transfer reactions and redox potentials of $[Co(bpy)_3]^{2+/3+}$ redox couples. In this article, geometrical and energetic characteristics of the complex in different oxidation states both in the gas phase and acetonitrile solvent (which is a common organic solvent in efficient DSCs) are presented. Furthermore, spectroscopic properties of the complexes in different media are calculated and analyzed. Based on the calculated energies and structural and electronic characteristics of both redox states of the complex in acetonitrile, an accurate Marcus diagram is derived for the electron-transfer reaction system $[Co(bpy)_3]^{2+}$ + $D35^+$/ $[Co(bpy)_3]^{3+}$ + D35. The experimental results obtained for a working DSC containing a mesoporous titania/D35 (a triarylamine dye) coated on fluorine doped tin oxide (FTO) as a working electrode, a platinum coated FTO as a counter electrode and an electrolyte medium with a $[Co(bpy)_3]^{2+/3+}$ redox couple are also presented and discussed.

2. Computational details

Full geometry optimization is carried out on the cobalt complexes by the density functional theory (DFT) method using a hybrid functional B3LYP.[34,35] The 6-31G(d,p) basis set is used for all atoms except for Co for which the LanL2DZ basis set[36] is used. This style of basis sets is abbreviated as 6-31G(d,p)[LanL2DZ]. Vibrational spectra (IR, Raman and vibrational circular dichroism (VCD)) have been computed for the optimized complexes using the same method and basis sets. Solvent effects on the structure and spectroscopic characteristics are evaluated by the conductor-like polarizable continuum model (CPCM)[37] using acetonitrile as solvent. All calculations are carried out using the Gaussion-09 quantum chemistry package[38] and its interface GaussView.[39]

The time-dependent DFT (TD-DFT) method has been applied to calculate the excited states of the complexes and their corresponding electronic transitions. The 50–50 and nstate = 7 keywords are used to request TD-DFT calculations for both spin states; doublet and quartet states for Co(II), and singlet and triplet states for Co(III). It should be noted here that computations carried out on the ground states of these complexes in both low spin and high spin states showed that the high spin and low spin states are the most stable states of the Co(II) and Co(III) complexes, respectively.

The Marcus diagram is derived for the electron transfer (ET) reaction system $[Co(bpy)_3]^{2+}$ + $D35^+$ / $[Co(bpy)_3]^{3+}$ + D35 in the CPCM modeled acetonitrile solvent using the scheme described below. A shifted parabolic behavior, as given by eqn (1), is assumed for both Co(II) and Co(III) oxidation states of the complex.

$$M_{II} = k_{II}(x - x_{II})^2 + M^0_{II},\ M_{III} = k_{III}(x - x_{III})^2 + M^0_{II} \qquad (1)$$

where II and III subscripts denote the Co(II) and Co(III) states, respectively. In these Marcus curves, the minimum energies are set to the shifted (by IR potential drop, 0.030 V) electronic energies M^0_{II} and M^0_{III} of the donor–acceptor pair before and after the ET process, respectively (*i.e.* $M^0_{II} = E^0$ (Co(II) + $D35^+$) + IR & $M^0_{III} = E^0$ (Co(III) + D35) + IR). With this definition, the energy change due to the electron transfer reaction (ET) is obtained as $\Delta E_{ET} = M^0_{II} - M^0_{III}$. Among a number of geometric parameters, only the average optimized Co–N bond length, R_{Co-N}, corresponding to the symmetric breathing mode of vibration of all six Co–N bonds of the $[Co(bpy)_3]$ complex represents the reaction coordinate x (with x_{II} = 2.170 & x_{III} = 1.964 Å). The force constants corresponding to this breathing vibrational mode obtained from vibrational analysis on the optimized structures are 1.9346 and 1.9560 mdyne $Å^{-1}$ for the Co(II) and Co(III) complexes, respectively. These values are scaled up by a factor of 67.1 to obtain a crossing point (the barrier energy) at R_c having an energy of $E_c = \Delta E_{ET} + V_{OC}$ (with V_{OC} = 0.820 V, measured experimentally). The values of the force constants appearing in eqn (1) are thus obtained as k_{II} = 129.81 & k_{III} = 131.24 eV $Å^{-2}$. The calculated Marcus diagram is demonstrated in Fig. 9. The structural changes observed for the acceptor system (dye@electrode) due to the ET process are small and can be ignored for this electron transfer analysis.

Duschinsky matrix elements,[40–42] connecting vibrational modes of the two Co(II) and Co(III) complexes, are calculated. Analysis of the Duschinsky matrix elements shows that the symmetric Co–N bond stretching (breathing) mode of vibration, involved in the ET reaction, remains 88.7% pure in the Co(II) → Co(III) conversion during ET reaction. The main contributing vibrational modes are the mode numbers 54, 53, and 49 having +6.94,

+5.93, and −17.31 cm^{-1} frequency difference ($\Delta\bar{\nu}$) from the breathing mode (*i.e.* mode number 52, appearing at 697.07 cm^{-1}), and 5.8%, 4.1%, and 0.3% contributions, respectively. Therefore, the ET from Co(II), and its conversion to Co(III), does not considerably mix the ET reaction coordinate with other vibrational modes of the complex. This validates the procedure used here to calculate the potential energy curves for derivation of the Marcus diagram.

3. Experimental details

3.1. Synthesis and cyclic voltammetry of the cobalt complex

The cobalt complex $[Co(bpy)_3](PF_6)_2$ is synthesized as described by Mosconi *et al.*,[43] Sapp *et al.*[44] and Klahr *et al.*[45] Briefly, 1 equivalent of $CoCl_2{\cdot}6H_2O$ and 3.3 equivalents of the polypyridine ligand are dissolved in a minimal amount of methanol (Merck), and the solution is stirred under reflux for 2 h. An excess of ammonium hexafluorophosphate is then added to the solution to precipitate the compound which is then filtered, washed with methanol and ethanol, dried under vacuum, and used without further purification.

Oxidation of the cobalt(II) complex is performed by adding a slight excess of $NOBF_4$ to an acetonitrile solution of the complex and then removing the acetonitrile solvent by rotary evaporation. The complex is then redissolved in acetonitrile, and a large amount of NH_4PF_6 is added to the solution. The final product was precipitated with diethyl ether, filtered, dried under vacuum, and used without further purification.

Cyclic voltammetry measurements are carried out on a 3 mM solution of the Co(II) complex in acetonitrile and 3-methoxy propionitrile with 0.1 M of tetrabutylammonium hexafluorophosphate as a supporting electrolyte using platinum, standard Ag/AgCl and 2 mm diameter glassy carbon electrodes as counter, reference and working electrodes, respectively (voltage scan rate is set to 50 mV s^{-1}).

3.2. Dye sensitized solar cell fabrication and characterization

A mesoporous titania working electrode with a thin layer of titania blocking layer is fabricated. The titania sol is prepared using a previously reported procedure.[46,47] For preparation of the working electrode, fluorine-doped tin oxide (FTO) glass substrates (Pilkington, TEC15) are cleaned in an ultrasonic bath overnight using sequentially detergent, water, and ethanol. The conducting glass substrates are coated in a dipping–withdrawing manner (withdrawing speed: 0.1 mm s^{-1}) (one layer) using titanium sol and preheated at 105 °C for 10 min. Mesoporous TiO_2 films are prepared with an area of 0.25 cm^2 by screen printing colloidal TiO_2 paste (Dyesol DSL 30 NRD-T) and preheating at 120 °C, then another time screen printing of scattering TiO_2 paste (PST-400C) and sintering. The temperature gradient program had four levels at 180 (10 min), 320 (10 min), 390 (10 min), and 500 °C (60 min).

After sintering, when the temperature cooled to about 90 °C, the electrode is immersed in a dye bath containing 0.2 mM D35 in ethanol and heated at 50 °C for 1 h. The film is then rinsed in ethanol to remove excess dyes. Solar cells are assembled, using a 30 μm thick thermoplastic Surlyn frame, with a platinized counter electrode (TEC8), prepared by depositing 10 μL cm^{-2}, 4.8 mM H_2PtCl_6 solution in ethanol onto the glass substrate followed by heating in air at 400 °C for 30 min. An electrolyte solution consisting of 0.22 M $[Co(bpy)_3](PF_6)_2$, 0.033 M $[Co(bpy)_3](PF_6)_3$, 0.1 M $LiClO_4$, and 0.2 M 4-*tert*-butylpyridine (TBP) in acetonitrile is then introduced through two holes predrilled in the counter electrode, and the cell is sealed using thermoplastic Surlyn covers and a glass cover slip.

Current–voltage (*I*–*V*) characteristics are measured using an Autolab potentiostat and a home-made solar simulator giving light with spectral distribution under AM1.5G conditions, which had been calibrated using a certified reference solar cell (Fraunhofer ISE) to an intensity of 1000 W m^{-2}. A black mask with an aperture slightly larger (0.6 × 0.6 cm^2) than the active area of the solar cell (0.5 × 0.5 cm^2) is applied on the top of the cell to avoid significant additional contribution from light falling on the device outside the active area.

4. Results and discussion

4.1. Photovoltaic results

Fig. 1 shows the photocurrent–voltage characteristics of the prepared DSC with the D35 dye in conjunction with the cobalt-based electrolyte under the 1 sun simulated sunlight (*i.e.* AM1.5G, 1000 W m^{-2}). The power conversion efficiency (PCE, η) is derived from this photocurrent–voltage plot using equation $\eta = J_{sc}V_{oc}FF/I_0$, where J_{sc} is the short-circuit current density, V_{oc} is the open-circuit voltage, FF is the fill factor, and I_0 is the photon flux illuminating the solar cell. The short-circuit current density and the open-circuit voltage of the DSC are measured to be 7.976 mA cm^{-2} and 820 mV, respectively. As reported in Fig. 1, a value of 4.4% is obtained for the PCE.

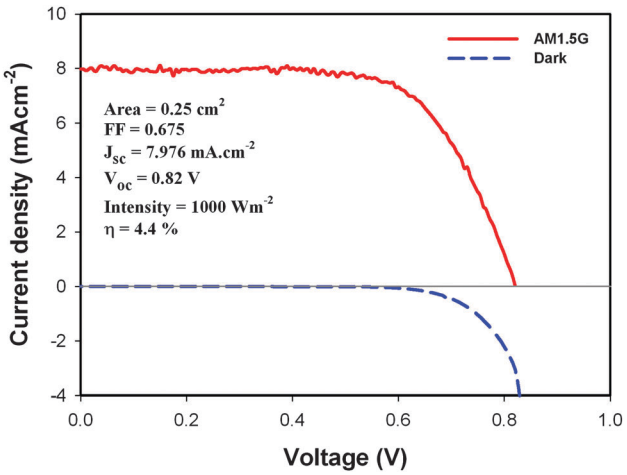

Fig. 1 Current density *versus* applied potential under dark (blue dash line) and AM1.5G illumination (red line) conditions obtained for the DSC sensitized with D35 in a $[Co(bpy)_3]^{2+/3+}$ redox couple based electrolyte system.

Analysis of the dark current of the prepared cell provides qualitative information about the electron recombination process.[48] In DSCs, preventing recapture of photo-injected electrons by redox species is vital to obtain a high open-circuit photo-voltage. By inserting a blocking layer between the FTO substrate and the TiO_2 mesoporous layer, the reaction possibilities of Co(II) complex species with the photo-injected electrons on the FTO substrate are significantly hindered, as demonstrated by the reduced dark current.[48] The dark current–voltage curve of the DSC using a titania blocking layer is presented in Fig. 1 (the blue dash line). The low dark current observed for this DSC may be attributed to the better electrical contact between the blocking layer and the FTO substrate, and the compact nature of the titania blocking layer as well.

4.2. Cyclic voltammograms of the cobalt complex

Electrochemical behavior of the $[Co(bpy)_3](PF_6)_2$ complex is investigated in acetonitrile and 3-methoxy propionitrile solutions using the cyclic voltammetry technique. The cyclic voltammograms are shown in Fig. 2. It can be seen from this figure that the CVs are well-behaved and the redox reaction is relatively reversible. The oxidation potentials for this complex (*i.e.* the $[Co(bpy)_3]^{2+} \rightarrow [Co(bpy)_3]^{3+}$ anodic electrochemical half-cycle) in acetonitrile and 3-methoxy propionitrile media are +0.40 V and +0.42 V, respectively. The energy difference between the two oxidation states of the $[Co(bpy)_3]$ complex calculated based on the TD-B3LYP/6-31G(d,p)[LanL2DZ] results is 0.59 eV which is close to these experimentally measured values. In the cathodic half-cycle, reduction reaction of the Co(III) center occurs at +0.27 V and +0.28 V in acetonitrile and 3-methoxy propionitrile, respectively. These data show that the redox potentials of the $[Co(bpy)_3](PF_6)_2$ complex in 3-methoxy propionitrile (frequently used solvent for DSC modules) are slightly higher because of higher polarity of this solvent in comparison to that of acetonitrile. Although the photocurrent observed in 3-methoxy propionitrile is lower due to its higher viscosity and lower mobilities of the ions, because of the practical limitations of the outdoor use of acetonitrile, *e.g.* its lower boiling point, this solvent is still preferred for DSC modules.

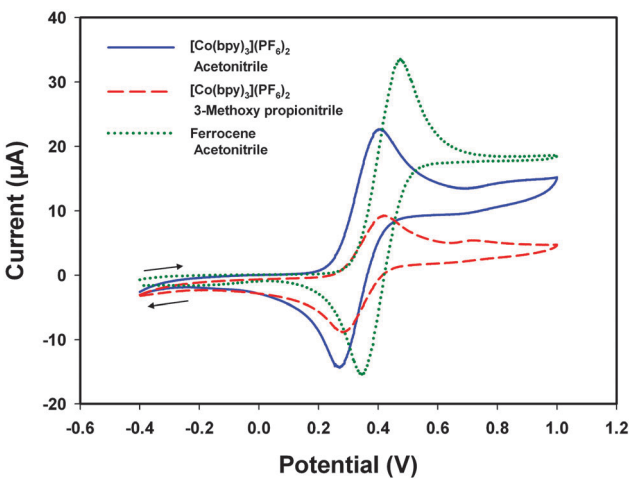

Fig. 2 Cyclic voltammograms (at a scan rate of 50 mV s^{-1}) recorded for the $[Co(bpy)_3](PF_6)_2$ complex in acetonitrile solution (blue solid line) and 3-methoxy propionitrile (red dashed line) and ferrocene in acetonitrile (green dotted line) for comparison. Platinum, Ag/AgCl standard and glassy carbon electrodes are used as counter, reference and working electrodes, respectively. The concentrations of the complexes and tetrabutylammonium hexafluorophosphate as a supporting electrolyte are set to 3 mM and 0.1 M, respectively.

4.3. Structures of the cobalt complexes

The typical B3LYP/6-31G(d,p)[LanL2DZ] optimized structure of both $[Co(bpy)_3]^{2+}$ and $[Co(bpy)_3]^{3+}$ complexes in the gas phase and acetonitrile is presented in Fig. 3a. The overall symmetry of these complexes, which have an octahedral (O_h) symmetry at the metal center, is D_3, and the Co(II) and Co(III) complexes have 3 and 0 single electrons in their d orbitals, thus having multiplicities of 4 and 1, respectively. Selected bond lengths and angles and the values of the D_3 symmetry characteristic angles β, γ, τ, and θ (as defined in Fig. 3b) in the optimized structures of these cobalt complexes are listed in Table 1. The (X-ray) experimental geometric parameters reported for tris(2,2′-bipyridine)-cobalt(II) diperchlorate[49] and tris(2,2′-bipyridine)-cobalt(III) triperchlorate dihydrate,[50] as the closest relative complex, are also included in Table 1 for comparison. The experimental values are averaged such that they can be compared to their corresponding calculated values in the D_3 symmetry.

A comparative analysis shows that values of the optimized geometric parameters calculated for the cobalt complexes compare well with the experimental values. This is, in particular, the case for the Co–N bond length. The 6-31G(p,d)[LanL2DZ] calculated Co–N bond lengths of the Co(II) complexes in the gas phase and acetonitrile medium are about 2.18 Å but the calculated Co–N bond length of Co(III) complexes is about 1.97 Å. These calculated geometric parameters give bond lengths which are slightly larger than the experimental values, which is due to the fact that the computational results correspond to the isolated molecules in the gas phase while the experimental results to the molecules in the solid state.

4.4. Frontier orbitals and electronic transitions

An electronic system with a larger HOMO–LUMO gap is expected to be less reactive than the one having a smaller gap.[51] The HOMO–LUMO gaps calculated for the Co(II) and Co(III) complexes in CPCM acetonitrile using the TD-B3LYP/6-31G(d,p)[LanL2DZ] method are 10.235 eV and 9.926 eV respectively.

The boundary surfaces of the HOMO and LUMO for the cobalt complexes in the gas phase and acetonitrile medium are shown in Fig. 4. The expansion coefficients of the HOMO and LUMO of the cobalt complexes in terms of basis functions of the 6-31G(p,d)[LanL2DZ] basis set are calculated and listed in Table 2. For $[Co(bpy)_3]^{2+}$ in the gas phase, the HOMO is localized by 29.6% of the d orbitals of the cobalt atom, 18.4% of p orbitals of nitrogen atoms (α spin) and 12.6% of p orbitals of carbon atoms (β spin), and the LUMO is mainly localized by 82.4% of d orbitals (with β spin) of cobalt and 12.5% of p orbitals (with α spin) on the carbon (6.2%) and nitrogen (6.3%) atoms of the bipyridine ligands. The orbital expansion

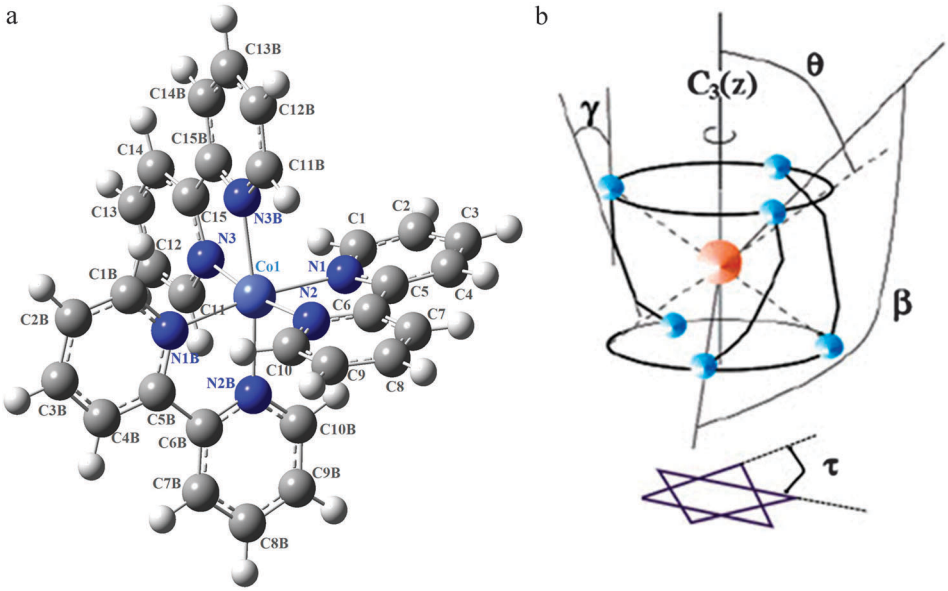

Fig. 3 (a) The optimized geometry of the cobalt complex obtained at the B3LYP/6-31G(d,p)[LanL2DZ] level of theory, and the numbering scheme used in this report. (b) The angles characterizing the arrangement of the ligands around the cobalt center: β is the N–Co–N angle, γ the dihedral angle between planes of the two rings of each ligand, τ the twist angle, and θ the angle between the z axis and the generator of the cone on which the nitrogen atoms are located.

coefficients obtained for the same Co(II) complex in acetonitrile show that the HOMO is more localized on the cobalt atom (46.7%) and contributions from the p orbitals of the carbon atoms is decreased to 4.2%, as compared to that in the gas phase.

Analysis of the frontier orbitals of the $[Co(bpy)_3]^{3+}$ complex shows that in both the gas phase and acetonitrile medium, the HOMO is localized mainly on the carbon atoms. The LUMO has contributions mainly from the cobalt atom (56.4% in the gas phase and 41.1% in acetonitrile) and nitrogen atoms of the bipyridine ligands (8.3% in the gas phase and 11.2% in acetonitrile).

Excitation parameters for the $[Co(bpy)_3]^{2+/3+}$ complexes are calculated using the TD-B3LYP/6-31G(p,d)[LanL2DZ] method and are listed in Table 3. Major contributions of the excited state of the $[Co(bpy)_3]^{2+}$ complex in both phases are mainly from the excitations from the HOMO, HOMO − 1 and HOMO − 2 to the LUMO, LUMO + 1 and LUMO + 2 of the ground state determinant. In terms of atomic contributions, excitations occur mainly from the d and p atomic orbitals of cobalt and nitrogen atoms (in the ground state) to the p atomic orbitals of nitrogen and carbon atoms (in the excitation state), so that this excitation can be considered as metal-to-ligand charge transfer (MLCT). The simulated UV-Vis spectra of the cobalt complexes are shown in Fig. 5. The major contributions of the Co(II) complex to the absorption spectrum appear at around 245 nm in the gas phase and 249 nm in acetonitrile. The excitation energy of these electron transitions is about 5 eV. The simulated UV-Vis spectra of Co(III) complexes have different peaks with different excitation energies. For this $[Co(bpy)_3]^{3+}$complex, there are three different excitation peaks at 257, 177 and 166 nm in the gas phase and four peaks at 262, 179, 174 and 168 nm in acetonitrile medium. These electronic transitions can be considered as ligand-to-metal electron transfer (LMCT). The frontier molecular orbital diagrams of the two $[Co(bpy)_3]^{2+/3+}$ complexes in the gas phase and acetonitrile are depicted in Fig. 6 where the electronic transitions producing the UV-Vis spectra are shown by colored arrows.

4.5. Infrared, Raman and VCD spectra of cobalt complexes

Vibrational analysis is carried out for both complexes, and their IR, Raman and vibrational circular dichroism (VCD) spectra are calculated using the same method used for structural optimization, and are reported in Table S1 (ESI†) where they are compared with the available experimental values.[52] The scaled (by a factor of 0.9614) B3LYP/6-31G(p,d)[LanL2DZ] vibrational frequencies of the complexes are in very good agreement with the experimental values.

Based on the D_3 symmetry of the two $[Co(bpy)_3]^{2+/3+}$ complexes, the normal vibrational modes with A_1, A_2 and E symmetries are Raman active, IR active and IR/Raman active, respectively. The calculated IR and Raman spectra of the $[Co(bpy)_3]^{2+/3+}$ complexes in the gas phase and acetonitrile medium are shown in Fig. 7. The vibrational modes of the Co(III) complex appear slightly at higher frequencies, as compared with those of the Co(II) complex. The strong IR peaks are related to the out-of-plane C–H bending and in-plane C–H bending combined with stretching of the C–C and C–N bonds. The in-plane ring and C–H bending, (C–C & C–N) and C–H bond stretching show higher Raman activity. The C–H stretching bands appearing at 3230–3315 cm^{-1} is a Raman active mode with A_1 symmetry. The Raman active A_1 modes of both cobalt tris-bipyridine complexes are polarized, but the E modes are depolarized.

The calculated VCD spectrum of the Co(II) and Co(III) complexes in the gas phase (Fig. 8) shows a strong peak at around 1040 cm^{-1} which is assigned to the in-plane ring and C–H bending mode. This mode is IR and Raman active and it could

Table 1 Selected B3LYP/6-31G(d,p)[LanL2DZ] optimized and X-ray experimental[46,47] geometrical parameters obtained for the $[Co(bpy)_3]^{2+}$ and $[Co(bpy)_3]^{3+}$ complexes (bond lengths in Å and angles in degrees)

	Exp. (X-ray)		B3LYP/6-31G(d,p)[LanL2DZ]			
			Co(II)		Co(III)	
Geometric parameter	Co(II)	Co(III)	Gas	Acetonitrile	Gas	Acetonitrile
Bond length						
Co1–N1	2.136	1.914	2.177	2.170	1.975	1.961
Co1–N2	2.133	1.937	2.177	2.169	1.975	1.964
Co1–N3	2.119	1.930	2.177	2.169	1.974	1.966
Co1–N1B	2.136	1.935	2.177	2.171	1.974	1.966
Co1–N2B	2.133	1.929	2.177	2.169	1.974	1.965
Co1–N3B	2.119	1.942	2.176	2.169	1.974	1.962
N1–C1	1.349	1.353	1.353	1.352	1.356	1.352
N1–C5	1.346	1.335	1.366	1.364	1.373	1.370
C1–C2	1.377	1.366	1.395	1.395	1.395	1.394
C2–C3	1.375	1.407	1.399	1.398	1.399	1.397
C3–C4	1.372	1.378	1.397	1.397	1.399	1.397
C4–C5	1.395	1.381	1.402	1.402	1.399	1.397
C5–C6	1.485	1.499	1.481	1.480	1.467	1.465
C6–C7	1.382	1.370	1.402	1.402	1.399	1.397
C7–C8	1.380	1.358	1.397	1.397	1.399	1.397
C8–C9	1.362	1.377	1.399	1.398	1.399	1.398
C9–C10	1.371	1.372	1.395	1.395	1.395	1.394
N2–C6	1.345	1.344	1.366	1.364	1.373	1.370
N2–C10	1.340	1.328	1.353	1.352	1.356	1.353
Bond angles						
N1–Co1–N2	77.1	83.1	76.2	76.3	82.7	83.1
N1–Co1–N3	95.4	93.9	97.7	97.7	94.7	94.8
N2–Co1–N3	171.4	175.3	171.6	171.7	176.4	177.1
N1–C5–C6	115.9	113.3	116.1	116.0	114.6	114.6
Torsion angles						
N1–C5–C6–N2	−5.7	3.2	−5.3	−4.30	−3.2	−3.8
C4–C5–C6–C7	−7.3	7.3	−5.9	−4.7	−2.8	−3.7
D_3 structure angles						
β	77.3	83.6	76.2	76.3	82.8	83.1
γ	3.3	4.1	4.0	3.3	2.3	2.6
τ	49.0	53.5	50.0	50.0	55.0	55.0
θ	53.0	43.0	61.0	61.0	59.0	58.5

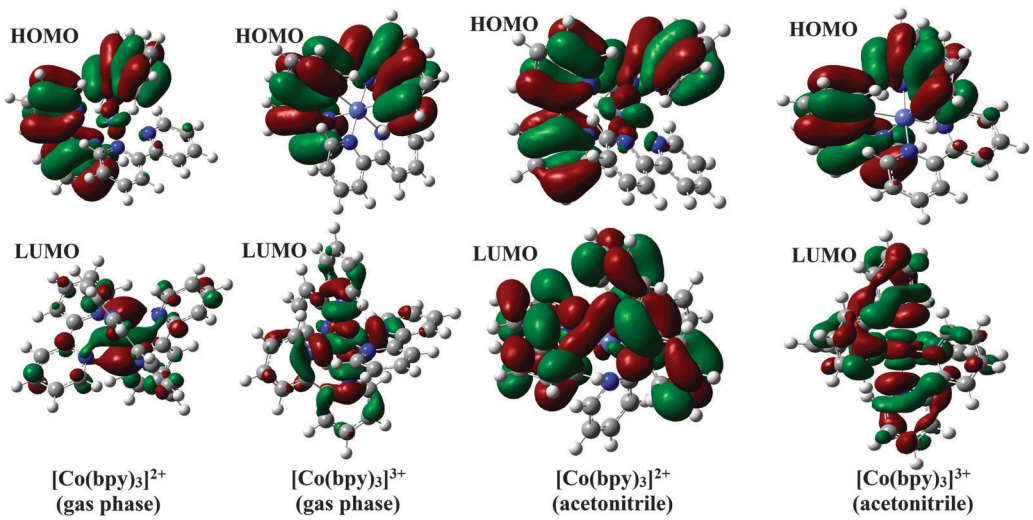

Fig. 4 The boundary surfaces of the HOMO and LUMO of the $[Co(bpy)_3]^{2+}$ and $[Co(bpy)_3]^{3+}$ complexes (in the gas phase and acetonitrile medium) obtained at the B3LYP/6-31G(d,p)[LanL2DZ] level of theory.

be attributed to one of the doubly degenerate E modes of the D_3 point group. Another strong band appears at 1497 cm^{-1} which is assigned to the combination of in-plane C–H bending with (C–N & C–C) stretching modes.

Table 2 Molecular orbital expansion coefficients of the HOMO and LUMO for α- and β-spin states of the cobalt complexes obtained at the B3LYP/6-31G(p,d)[LanL2DZ] level of theory

Medium	Complex	Molecular orbital	Energy (Hartree)	Coefficients of Mos
Gas phase	$[Co(bpy)_3]^{2+}$	HOMO	−0.44204	α-Spin: 14.6% $7d_{-1}$(Co55) + 12.3% $7d_{-2}$(Co55) − 6.4% $2p_y$(N61) + 4.4% $2p_y$(N60) − 4.3% $2p_x$(N58) + 3.3% $2p_y$(N58)
			−0.45106	β-Spin: 2.9% $2p_x$(C49) − 2.8% $2p_x$(C39) + 2.7% $7d_{+2}$(Co55) + 2.4% $2p_x$(C43) − 2.3% $2p_x$(C45) − 2.2% $2p_x$(C44)
		LUMO	−0.27310	α-Spin: 2.2% $2p_y$(N57) + 2.1% $2p_z$(C10) − 2.1% $2p_z$(N56) + 2.1% $2p_z$(C9) − 2.0% $2p_z$(N57) − 2.0% $2p_y$(C10)
			−0.27289	β-Spin: 63.5% $7d_0$(Co55) + 18.9% $8d_0$(Co55)
	$[Co(bpy)_3]^{3+}$	HOMO	−0.57375	α/β-Spins: 2.5% $2p_y$(C33) − 2.3% $2p_y$(C21) − 2.2% $2p_x$(C15) − 2.2% $2p_y$(C29) + 2.2% $2p_x$(C3) − 2.1% $2p_y$(C28)
		LUMO	−0.41058	α/β-Spins: 38.7% $7d_{+1}$(Co55) + 16.9% $7d_{-2}$(Co55) − 3.3% $2p_x$(N58) + 3.2% $2p_x$(N61) + 1.8% $2p_x$(N59) + 1.8% $7d_{+2}$(Co55)
Acetonitrile	$[Co(bpy)_3]^{2+}$	HOMO	−0.25912	α-Spin: 18.1% $7d_{+1}$(Co55) + 12.8% $7d_{-2}$(Co55) − 6.0% $2p_x$(N59) + 5.9% $2p_x$(N58) − 3.3% $2p_x$(N61) + 3.3% $2p_x$(N57)
			−0.27101	β-Spin: 5.8% $7d_{-1}$(Co55) − 5.5% $7d_{+2}$(Co55) − 2.5% $7d_{-2}$(Co55) + 2.1% $2p_y$(C21) − 2.1% $2p_y$(C33) + 2.0% $7d_{+1}$(Co55)
		LUMO	−0.09342	α-Spin: 2.2% $2p_x$(N61) + 2.0% $2p_x$(N60) + 2.0% $2p_x$(N57) − 1.8% $2p_x$(C43) − 1.8% $2p_x$(C44) + 1.8% $2p_x$(N56)
			−0.09268	β-Spin: 2.6% $2p_x$(N57) + 2.2% $2p_x$(N61) + 2.0% $2p_x$(N56) + 1.8% $2p_z$(C10) − 1.8% $2p_x$(C10) + 1.8% $7d_{-1}$(Co55)
	$[Co(bpy)_3]^{3+}$	HOMO	−0.29432	α/β-Spins: 2.4% $2p_x$(C39) − 2.4% $2p_x$(C49) − 2.2% $2p_x$(C41) − 2.1% $2p_z$(C49) + 2.1% $2p_z$(C39) + 2.1% $2p_x$(C45)
		LUMO	−0.12706	α/β-Spins: 30.6% $7d_{+1}$(Co55) − 10.5% $7d_{-2}$(Co55) + 3.8% $2p_x$(N60) − 2.6% $2p_x$(N56) − 2.5% $2p_y$(N56) − 2.3% $2p_y$(N57)

Table 3 The TD-B3LYP/6-31G(p,d)[LanL2DZ] spectroscopic excitation parameters obtained for the $[Co(bpy)_3]^{2+}$ and $[Co(bpy)_3]^{3+}$ complexes (H and L denote HOMO and LUMO, respectively)

Medium	Complex	λ (nm)	Δ*E* (eV)	Oscillator strength	Symmetry	Major contributions
Gas phase	$[Co(bpy)_3]^{2+}$	245	5.060	0.65	^4A	H − 2(A) → L + 2(A) (13%), H − 1(A) → L(A) (14%), H(A) → L + 1(A) (14%), H − 2(B) → L + 2(B) (13%), H − 1(B) → L(B) (15%), H(B) → L + 1(B) (15%)
	$[Co(bpy)_3]^{3+}$	257	4.824	0.61	^1A	H − 2 → L + 2 (23%), H − 1 → L (31%), H → L + 1 (31%)
		177	7.001	0.51	^1A	H − 4 → L (17%), H − 3 → L + 1 (17%), H − 2 → L + 3 (12%)
		166	7.466	0.84	^1A	H − 5 → L (11%)
Acetonitrile	$[Co(bpy)_3]^{2+}$	249	4.979	0.88	^4A	H − 2(A) → L + 2(A) (13%), H − 1(A) → L(A) (10%), H(A) → L + 1(A) (10%), H − 2(B) → L + 2(B) (13%), H − 1(B) → L(B) (13%), H(B) → L + 1(B) (13%)
	$[Co(bpy)_3]^{3+}$	262	4.734	0.85	^1A	H − 2 → L + 2 (24%), H − 1 → L (32%), H → L + 1 (29%)
		179	6.929	0.57	^1A	H − 4 → L + 1 (10%), H − 3 → L (10%), H − 2 → L + 3 (10%)
		174	7.136	0.69	^1A	H − 2 → L + 1 (25%), H − 1 → L (19%), H → L + 1 (18%)
		168	7.380	0.97	^1A	H − 2 → L (30%), H − 1 → L + 2 (48%)

4.6. Marcus diagram

In the scheme used to derive Marcus diagram, the apparent activation energy of the $[Co(bpy)_3]^{2+}$ + $D35^+$ → $[Co(bpy)_3]^{3+}$ + D35 electron transfer reaction is assumed to be V_{oc} (Fig. 9). A MM+ optimized structure of this donor–acceptor system at the TiO_2 surface is shown in Fig. 10.

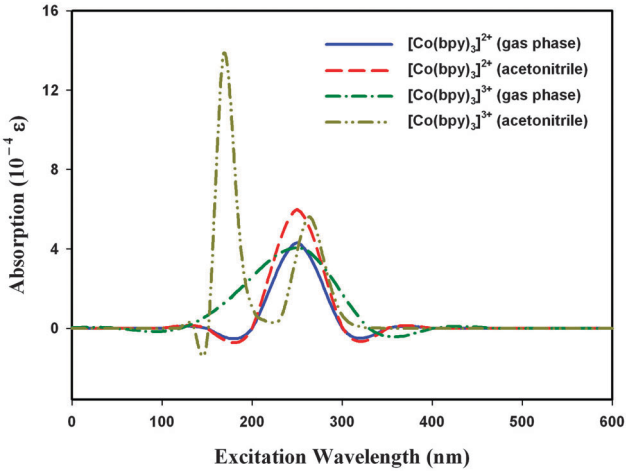

Fig. 5 The UV-Vis spectra simulated for the cobalt complexes using the TD-B3LYP/6-31G(d,p)[LanL2DZ] method.

The combined theoretical and experimental energy data show that the reactants are prepared at energies much higher than the energy of the crossing point at R_c (*i.e.* E_c, in Fig. 9). According to Marcus–Hush ET theory, the effective activation energy of the ET reaction is defined as:

$$\Delta E_{ET}{}^{*} = \frac{(\lambda + \Delta E_{ET})^2}{4\lambda} \qquad (2)$$

where λ is the reorganization energy and ΔE_{ET} is the energy difference between the products and reactants in their equilibrium geometries.[53] The reorganization energy (λ) has been calculated as the single-point energy of the product $[Co(bpy)_3]^{3+}$ + D35 at the equilibrium ground state geometry of the reactant $[Co(bpy)_3]^{2+}$ + $D35^{+}$, referenced to its energy at its own ground state equilibrium geometry. In acetonitrile medium, ΔE_{ET} = −1.264 eV, and the reorganization energy is calculated to be λ = 5.482 eV using eqn (1). Therefore, using eqn (2), a value of 0.811 eV can be assigned to the effective ET activation energy (ΔE_{ET}*) of the $[Co(bpy)_3]^{2+}$ + $D35^{+}$ donor–acceptor system. These values show that the ET reaction of this system in acetonitrile medium occurs in the Marcus normal region ($-\Delta E_{ET} < \lambda$), and that this system is appropriate for DSC application.

De Angelis and co-workers calculated reorganization energies for regeneration of electron transfer by a series of cobalt complexes and a number of dyes. Using an equilibrium solvation assumption, they determined λ-values of about 0.6 and 1.4 eV for regeneration by cobalt complexes in the low and high spin states, respectively. For non-equilibrium solvation, an additional 0.6 eV in λ is calculated.[54] Boschloo and co-workers investigated the regeneration and recombination kinetics of dye-sensitized solar cells (DSCs) using a series of different cobalt polypyridine redox couples, with redox potentials ranging between 0.34 and 1.20 V (*vs.* NHE) and they applied Marcus theory to explain the rate of electron transfer.[55] They found that the regeneration kinetics for a number of different dyes (L0, D35, Y123, and Z907) by most of the examined cobalt redox shuttles occurs in the Marcus normal region. The calculated reorganization energies for the regeneration reaction range between 0.59 and 0.70 eV for different organic and organometallic dyes. Under the experimental conditions, the regeneration efficiency decreases with cobalt complexes having redox potentials of 0.4 eV or less.

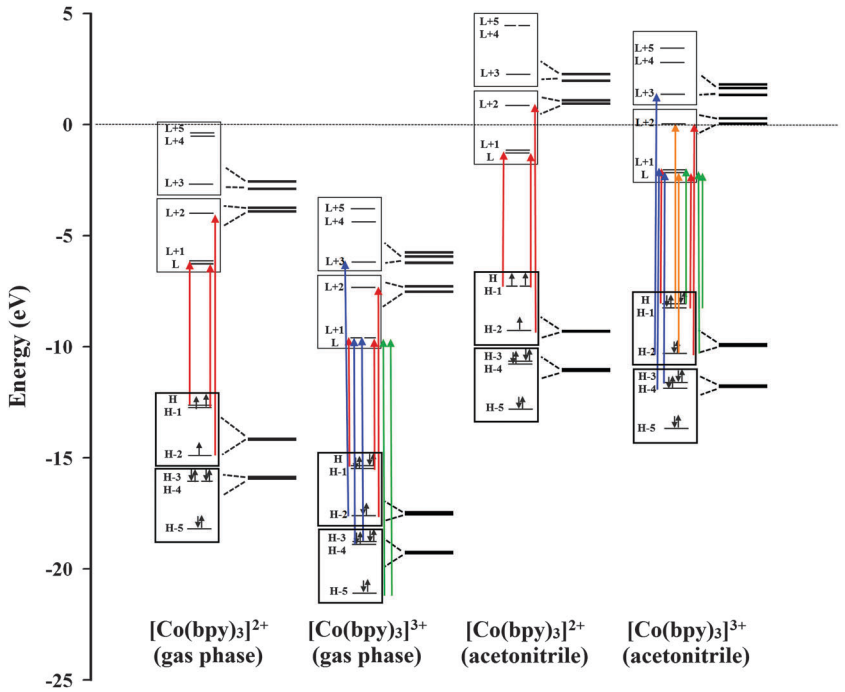

Fig. 6 The frontier occupied and virtual molecular orbital energy levels calculated for the $[Co(bpy)_3]^{2+}$ and $[Co(bpy)_3]^{3+}$ complexes in the gas phase and acetonitrile medium using the TD-B3LYP/6-31G(d,p)[LanL2DZ] method. Electronic transitions are shown by colored arrows.

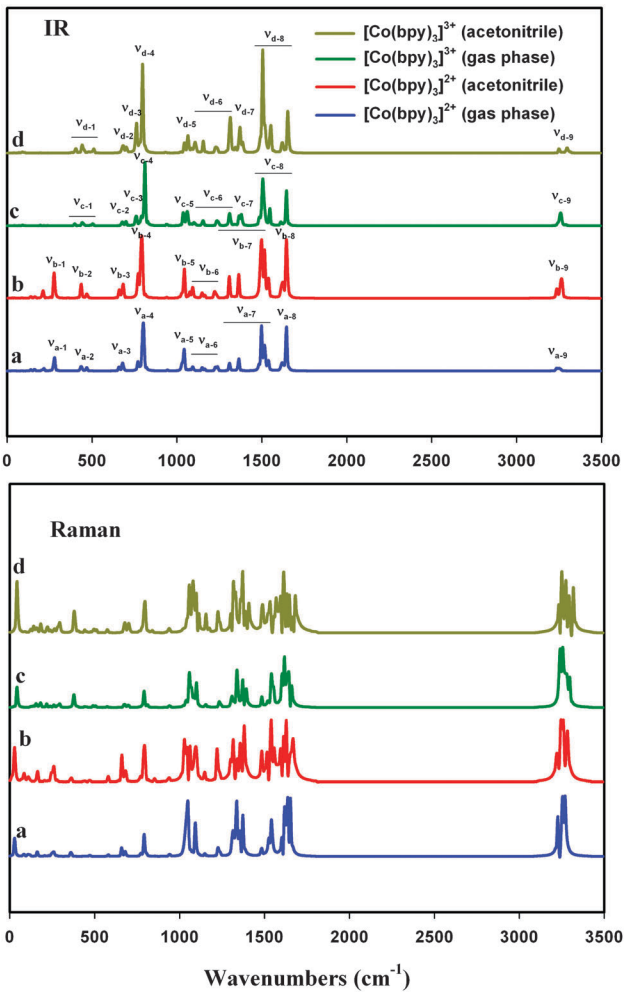

Fig. 7 Simulated IR (a) and Raman (b) spectra of the $[Co(bpy)_3]^{2+}$ and $[Co(bpy)_3]^{3+}$ complexes. Selected vibrational bands are assigned as (see Table S1, ESI†): ν_{a1} & ν_{b1}, ν_{Co-N} stretching; ν_{a2} & ν_{b2}, out-of-plane ring C–H bending; ν_{a3} & ν_{b3}, φ_{C-C}, φ_{C-N} torsion; ν_{a4} & ν_{b4}, γ_{C-H} in-plane C–C–H bending; ν_{a5} & ν_{b5}, in-plane ring and C–H bending; ν_{a6} & ν_{b6}, in-plane C–H bending; ν_{a7} & ν_{b7}, ν_{C-C} & ν_{C-N} stretching and in-plane C–H bending; ν_{a8} & ν_{b8}, ν_{C-C} stretching; ν_{a9} & ν_{b9}, ν_{C-H} stretching; ν_{c1} & ν_{d1}, ν_{Co-N} stretching and N–Co–N bending; ν_{c2} & ν_{d2}, in-plane ring C–H bending; ν_{c3} & ν_{d3}, out-of-plane ring C–H bending; ν_{c4} & ν_{d4}, γ_{C-H} in-plane C–H bending; ν_{c5} & ν_{d5}, in-plane ring bending; ν_{c6} & ν_{d6}, in-plane ring and C–H bending; ν_{c7} & ν_{d7}, in-plane C–H bending; ν_{c8} & ν_{d8}, ν_{C-C}, ν_{C-N} stretching and in-plane C–H bending; ν_{c9} & ν_{d9}, ν_{C-H} stretching.

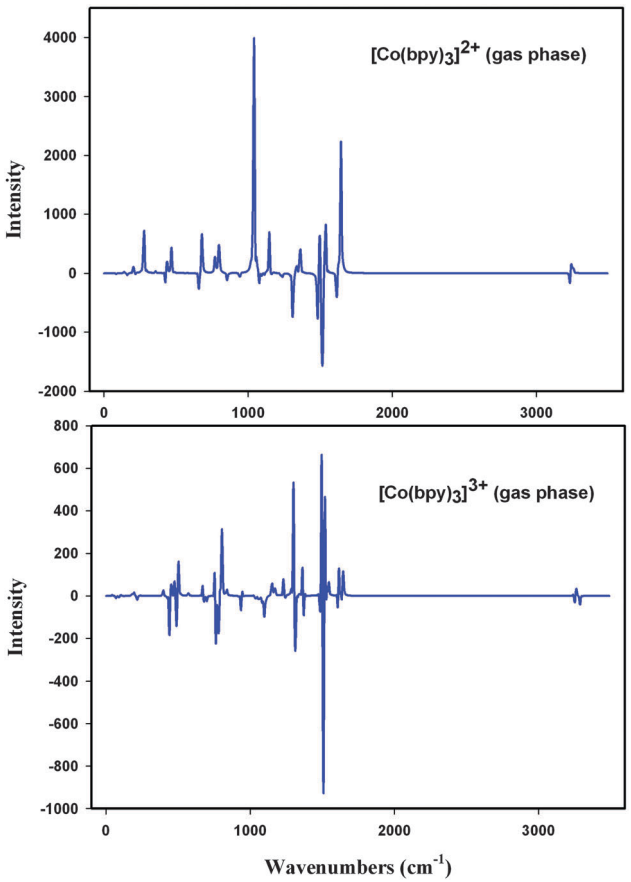

Fig. 8 Simulated vibrational circular dichroism (VCD) spectra of the $[Co(bpy)_3]^{2+}$ and $[Co(bpy)_3]^{3+}$ complexes in the gas phase using B3LYP/6-31G(p,d)[LanL2DZ].

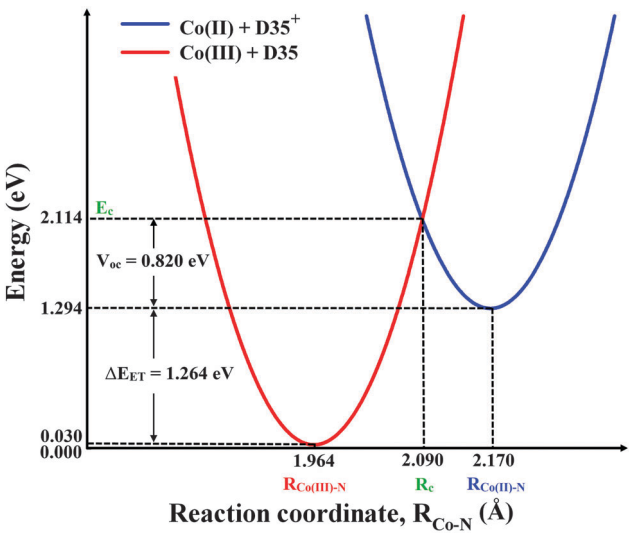

Fig. 9 Marcus diagrams derived for the electron transfer reaction of the $[Co(bpy)_3]^{2+}$ + $D35^+$ / $[Co(bpy)_3]^{3+}$ + D35 redox system in acetonitrile medium.

It is also found that the dark current decreases for cobalt complexes with highly positive redox potentials (above 0.55 V *vs.* NHE), which is consistent with electron transfer reactions occurring in the Marcus inverted region.[56] It can thus be concluded that the electron transfer energetics obtained with the R_{Co-N} coordinate based on the analysis of the Marcus diagrams in the present work are reliable.

5. Conclusions

We have reported a combined experimental and computational investigation to understand the nature of the electron transfer reactions between cobalt(II) and cobalt(III) redox mediators in dye-sensitized solar cells. The theoretical DFT calculations of the vibrational and electronic spectra of the cobalt complexes

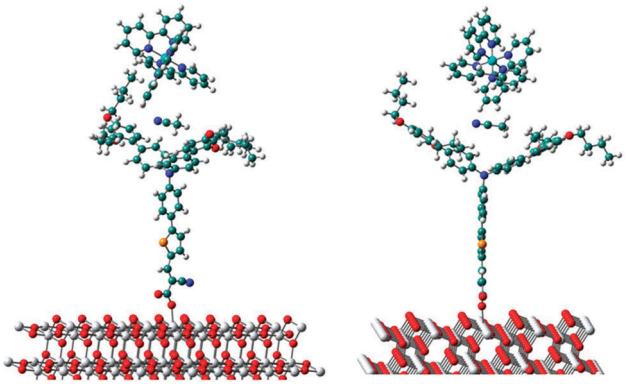

Fig. 10 Configuration of D35@TiO_2 and the accompanying $Co[(bpy)_3]^{2+/3+}$ complex mediated by a layer of acetonitrile solvent molecules (one of which is shown here).

were calculated and the results were compared with the experimental vibrational spectrum of cobalt(II)-tris-bipyridine in a high spin state. High intensity IR peaks are related to out-of-plane CH bending and in-plane CH bending combined with stretching of CC and CN bonds. In-plane ring and CH bending, CC and CN bond stretching and CH bond stretching show higher intensity Raman peaks in comparison with other vibrational modes. The calculated VCD peak at around 1040 cm^{-1}, which is assigned to in-plane ring and CH bending, is very intense compared to the observed transitions. Calculation of the atomic orbital coefficients of the frontier molecular orbitals (HOMO and LUMO) of the cobalt complexes shows that atomic orbitals which contribute to the HOMO of $[Co(bpy)_3]^{3+}$ are localized mainly on carbon atoms while those of the HOMO of $[Co(bpy)_3]^{2+}$ are localized on cobalt and nitrogen atoms. Furthermore, the LUMOs of Co(II) complex are also mainly on the carbon and nitrogen atoms but the LUMO of the Co(III) complex is mainly on the cobalt and nitrogen atoms. Therefore, calculated electronic transitions of the Co(II) complex are mainly derived from metal to ligand charge transfer (MLCT) and calculated electronic transitions of the Co(III) complex are mainly derived from ligand to metal charge transfer (LMCT). The energetics of the electron transfer process estimated based on Marcus theory considering R_{Co-N} as a reaction coordinate is compatible with what is reported in the literature based on experimental and computational studies.

Acknowledgements

We gratefully thank our colleague Meiyuan Guo for sharing his experience in computing. The computations are performed on resources provided by SNIC through Uppsala Multidisciplinary Center for Advanced Computational Science (UPPMAX) under the project p2011174.

References

1 B. O'Regan and M. Grätzel, *Nature*, 1991, **353**, 737.
2 A. Hagfeldt, G. Boschloo, L. Sun, L. Kloo and H. Pettersson, *Chem. Rev.*, 2010, **110**, 6595.
3 G. Boschloo, J. Lindström, E. Magnussom, A. Holmberg and A. Hagfeldt, *J. Photochem. Photobiol., A*, 2002, **148**, 11.
4 M. Nazeeruddin, A. Kay, I. Rodicio, R. Humphry-Baker, E. Muller, P. Liska, N. Vlachopoulos and M. Grätzel, *J. Am. Chem. Soc.*, 1993, **115**, 6382.
5 S. M. Feldt, E. A. Gibson, E. Gabrielsson, L. Sun, G. Boschloo and A. Hagfeldt, *J. Am. Chem. Soc.*, 2010, **132**, 16714.
6 K. M. Lee, V. Suryanarayanan and K. C. Ho, *J. Power Sources*, 2009, **188**, 635.
7 H. Liyuan, I. Ashraful, C. Han, M. Chandrasekharam, C. Barreddi, Z. Shufang, Y. Xudong and Y. Masatoshi, *Energy Environ. Sci.*, 2012, **5**, 6057.
8 W. Zeng, Y. Cao, Y. Bai, Y. Wang, Y. Shi, M. Zhang, F. Wang, C. Pan and P. Wang, *Chem. Mater.*, 2010, **22**, 1915.
9 J. G. Rowley, B. H. Farnum, S. Ardo and G. J. Meyer, *J. Phys. Chem. Lett.*, 2010, **1**, 3132.
10 G. Boschloo and A. Hagfeldt, *Acc. Chem. Res.*, 2009, **42**, 1819.
11 F. Matar, T. H. Ghaddar, K. Walley, T. DosSantos, J. R. Durrant and B. O'Regan, *J. Mater. Chem.*, 2008, **18**, 4246.
12 M. Wang, N. Chamberland, L. Breau, J.-E. Moser, R. H. Baker, B. Marsan, S. M. Zakeeruddin and M. Grätzel, *Nat. Chem.*, 2010, **2**, 385.
13 D. Li, H. Li, Y. Luo, K. Li, Q. Meng, M. Armand and L. Chen, *Adv. Funct. Mater.*, 2010, **20**, 3358.
14 T. Daeneke, T.-H. Kwon, A. B. Holmes, N. W. Duffy, U. Bach and L. Spiccia, *Nat. Chem.*, 2011, **3**, 211.
15 M. H. Habibi, A. H. Habibi, M. Zendehdel and M. Habibi, *Spectrochim. Acta, Part A*, 2013, **110**, 226.
16 M. H. Habibi, M. Mikhak, M. Zendehdel and M. Habibi, *Int. J. Electrochem. Sci.*, 2012, **7**, 6787.
17 M. H. Habibi, E. Askari, M. Habibi and M. Zendehdel, *Spectrochim. Acta, Part A*, 2013, **104**, 197.
18 A. Yella, H. W. Lee, H. N. Tsao, C. Yi, A. K. Chandiran, M. K. Nazeeruddin, E. W. G. Diau, C. Y. Yeh, S. M. Zakeeruddin and M. Grätzel, *Science*, 2011, **334**, 629.
19 A. Vargas, M. Zerara, E. Krausz, A. Hauser and L. M. L. Daku, *J. Chem. Theory Comput.*, 2006, **2**, 1342.
20 I. Krivokapic, M. Zerara, M. L. Dakua, A. Vargas, C. Enachescu, C. Ambrusc, P. Tregenna-Piggott, N. Amstutz, E. Krausz and A. Hauser, *Coord. Chem. Rev.*, 2007, **251**, 364.
21 K. Mizuno and J. H. Lunsford, *Inorg. Chem.*, 1983, **22**, 3484.
22 S. K. Tiwary and S. Vasudevan, *Chem. Phys. Lett.*, 1997, **277**, 84.
23 S. K. Tiwary and S. Vasudevan, *Inorg. Chem.*, 1998, **37**, 5239.
24 R. Sieber, S. Decurtins, H. Stoeckli-Evans, C. Wilson, D. Yufit, J. A. K. Howard, S. C. Capelli and A. Hauser, *Chem. – Eur. J.*, 2000, **6**, 361.
25 M. Zerara and A. Hauser, *ChemPhysChem*, 2004, **5**, 395.
26 M. D. Newton, *Coord. Chem. Rev.*, 2003, **238**, 167.
27 R. A. Marcus, *J. Chem. Phys.*, 1956, **24**, 966.
28 M. D. Newton and N. Sutin, *Annu. Rev. Phys. Chem.*, 1984, **35**, 437.
29 J. F. Endicott, X. Song, M. A. Watzky and T. Buranda, *J. Photochem. Photobiol., A*, 1994, **82**, 181.
30 A. Yoshimura, Md. J. Uddin, N. Amasaki and T. Ohno, *J. Phys. Chem. A*, 2001, **105**, 10846.

31 E. Mosconi, J.-H. Yum, F. Kessler, C. J. Gomez Garcia, C. Zuccaccia, A. Cinti, M. K. Nazeeruddin, M. Grätzel and F. De Angelis, *J. Am. Chem. Soc.*, 2012, **134**, 19438.
32 M. D. Newton, *J. Phys. Chem.*, 1986, **90**, 3734.
33 M. D. Newton, *J. Phys. Chem.*, 1991, **95**, 30.
34 A. D. Becke, *J. Chem. Phys.*, 1993, **98**, 5648.
35 C. Lee, W. Yang and R. G. Parr, *Phys. Rev. B: Condens. Matter Mater. Phys.*, 1988, **37**, 785.
36 W. J. Hehre, L. Rado, P. V. R. Scheleyer and J. A. Pople, *Ab initio Molecular Orbital Theory*, Wiley, New York, 1986.
37 M. Cossi, N. Rega, G. Scalmani and V. Barone, *J. Comput. Chem.*, 2003, **24**, 669.
38 M. J. Frisch, G. W. Trucks, H. B. Schlegel, G. E. Scuseria, M. A. Robb, J. R. Cheeseman, G. Scalmani, V. Barone, B. Mennucci, G. A. Petersson, H. Nakatsuji, M. Caricato, X. Li, H. P. Hratchian, A. F. Izmaylov, J. Bloino, G. Zheng, J. L. Sonnenberg, M. Hada, M. Ehara, K. Toyota, R. Fukuda, J. Hasegawa, M. Ishida, T. Nakajima, Y. Honda, O. Kitao, H. Nakai, T. Vreven, J. A. Montgomery Jr., J. E. Peralta, F. Ogliaro, M. Bearpark, J. J. Heyd, E. Brothers, K. N. Kudin, V. N. Staroverov, R. Kobayashi, J. Normand, K. Raghavachari, A. Rendell, J. C. Burant, S. S. Iyengar, J. Tomasi, M. Cossi, N. Rega, J. M. Millam, M. Klene, J. E. Knox, J. B. Cross, V. Bakken, C. Adamo, J. Jaramillo, R. Gomperts, R. E. Stratmann, O. Yazyev, A. J. Austin, R. Cammi, C. Pomelli, J. W. Ochterski, R. L. Martin, K. Morokuma, V. G. Zakrzewski, G. A. Voth, P. Salvador, J. J. Dannenberg, S. Dapprich, A. D. Daniels, O. Farkas, J. B. Foresman, J. V. Ortiz, J. Cioslowski and D. J. Fox, *Gaussian 09, Revision A.1*, Gaussian, Inc., Wallingford, CT, 2009.
39 *GaussView 03*, Gaussian Inc., Pittsburg, PA 15106, USA.
40 H. J. Kupka, *Transitions in Molecular Systems*, Wiley-VCH, Weinheim, 2010.
41 T. I. Yacovitch, J. B. Kim, E. Garand, D. G. van der Poll and D. M. Neumark, *J. Chem. Phys.*, 2011, **134**, 134307.
42 J. Huh, PhD thesis, *Unified description of vibronic transitions with coherent states*, Johann Wolfgang Goethe University, 2010.
43 E. Mosconi, J.-H. Yum, F. Kessler, C. J. Gomez Garcia, C. Zuccaccia, A. Cinti, M. K. Nazeeruddin, M. Grätzel and F. De Angelis, *J. Am. Chem. Soc.*, 2012, **134**, 19438.
44 S. A. Sapp, C. M. Elliott, C. Contado, S. Caramori and C. A. Bignozzi, *J. Am. Chem. Soc.*, 2002, **124**, 11215.
45 B. M. Klahr and T. W. Hamann, *J. Phys. Chem. C*, 2009, **113**, 14040.
46 M. H. Habibi and M. Zendehdel, *Curr. Nanosci.*, 2010, **6**, 642.
47 M. H. Habibi and M. Zendehdel, *J. Inorg. Organomet. Polym.*, 2011, **21**, 634.
48 S. Ito, P. Liska, R. Charvet, P. Pechy, U. Bach, L. Schmidt-Mende, S. M. Zakeeruddin, A. Kay, M. K. Nazeeruddin and M. Grätzel, *Chem. Commun.*, 2005, 4351.
49 J.-C. Yao, L.-F. Ma and F.-J. Yao, *Z. Kristallogr. – New Cryst. Struct.*, 2005, **220**, 483.
50 M. Du, X.-J. Zhao and H. Cai, *Z. Kristallogr. – New Cryst. Struct.*, 2004, **219**, 463.
51 R. Kurtaran, S. Odabas Ôglu, A. Azizoglu, H. Kara and O. Atakol, *Polyhedron*, 2007, **26**, 5069.
52 R. G. Inskeep, *J. Inorg. Nucl. Chem.*, 1962, **24**, 763.
53 R. A. Marcus, *J. Chem. Phys.*, 1956, **24**, 966.
54 E. Mosconi, J.-H. Yum, F. Kessler, C. J. Gomez-Garcia, C. Zuccaccia, A. Cinti, M. K. Nazeeruddin, M. Grätzel and F. De Angelis, *J. Am. Chem. Soc.*, 2012, **134**, 19438.
55 S. M. Feldt, P. W. Lohse, F. Kessler, M. K. Nazeeruddin, M. Gratzel, G. Boschloo and A. Hagfeldt, *Phys. Chem. Chem. Phys.*, 2013, **15**, 7078.
56 T. P. Gerasimova and S. A. Katsyuba, *Dalton Trans.*, 2013, **42**, 1787.